Available online at www.sciencedirect.com
ScienceDirect
Chemical Geology 246 (2007) 19–38
CHEMICAL GEOLOGY INCLUDING ISOTOPE GEOSCIENCE
www.elsevier.com/locate/chemgeo

Modeling the carbon and sulfur isotope compositions of marine sediments: Climate evolution during the Devonian

Laurent Simon [a], Yves Goddéris [b,*], Werner Buggisch [a], Harald Strauss [c], Michael M. Joachimski [a]

[a] *Institut für Geologie und Mineralogie, Universität Erlangen-Nürnberg, Schlossgarten 5, 91054 Erlangen, Germany*
[b] *LMTG, Observatoire Midi Pyrénées, CNRS–Université de Toulouse, 14 av. Édouard Belin, 31400 Toulouse, France*
[c] *Geologisch-Paläontologisches Institut, Westfälische Wilhelms Universität, Corrensstr. 24, 48149 Münster, Germany*

Received 28 March 2007; received in revised form 30 August 2007; accepted 31 August 2007

Editor: B. Bourdon

Abstract

A model of global biogeochemical cycles coupled to an energy-balance climatic model (modified after the COMBINE model; [Goddéris, Y., Joachimski, M.M., 2004. Global change in the Late Devonian: modeling the Frasnian–Famennian short-term carbon isotope excursions. Palaeogeogr. Palaeoclimatol. Palaeoecol. 202, 309–329]) is used to calculate the short-term evolution of atmospheric pCO_2 during the Devonian. The geochemical cycles for carbon, alkalinity, phosphorus, sulfur and oxygen are included in this model, with also ^{13}C and ^{34}S cycles. High-resolution records of $\delta^{13}C$ of marine carbonates and $\delta^{34}S$ of marine sulfates are used as forcing parameters of the geochemical cycles in an inverse modeling. Atmospheric pCO_2 and pO_2 at the end of the Silurian are calculated to have been 3000 ppmv and 0.165 bar (0.75 PAL), respectively. A long-term decrease in pCO_2 is modeled for almost the entire Devonian. Short-term lowering of pCO_2 to concentrations around 2000 ppmv is calculated for the Silurian–Devonian transition and the Pragian. Contents around 900 ppmv are modeled for the Eifelian–Givetian, Givetian–Frasnian and Frasnian–Famennian boundaries as a consequence of enhanced organic carbon burial during deposition of Lochkovian, Eifelian, and Frasnian grey and black shales. Organic carbon burial is enhanced by the increase of phosphorus delivery to the ocean triggered by short-term sea-level falls. The corresponding short-term global climatic cooling at the Silurian–Devonian boundary, at the end of the Pragian, and the Givetian–Frasnian as well as Frasnian–Famennian boundaries reached 2 °C at the equator. The rapid colonization of continental surface by land plants during the Middle and Late Devonian, increasing chemical alteration of the continents and CO_2 consumption by silicate weathering, is assumed to have caused cooling of surface seawater, as suggested by the $\delta^{18}O$ values of biogenic apatites.
© 2007 Elsevier B.V. All rights reserved.

Keywords: Modeling; Carbon; Sulfur; Isotope ratios; Carbon dioxide; Devonian

1. Introduction

Major environmental changes took place during the Devonian which strongly affected the biosphere. Important biotic crises occurred during the Devonian (Sepkoski, 1996; Walliser, 1996), among which the Frasnian–

* Corresponding author. Present address: LMTG, 14 avenue E. Belin, 31400, Toulouse, France.
E-mail address: godderis@lmtg.obs-mip.fr (Y. Goddéris).

0009-2541/$ - see front matter © 2007 Elsevier B.V. All rights reserved.
doi:10.1016/j.chemgeo.2007.08.014

Famennian mass extinction event had a major impact on the tropical marine ecosystem. Evidence for the development of ice sheets in South America exists for the Late Famennian (Streel et al., 2000). Various mechanisms have been proposed as causes of the Devonian mass extinction events: climate warming (Thompson and Newton, 1988; Ormiston and Oglesby, 1995), or cooling (Joachimski and Buggisch, 2002), global oceanic anoxia (Buggisch, 1991; Joachimski and Buggisch, 1993; Murphy et al., 2000), the colonization of continents by vascular plants (Algeo et al., 1995), increased mountain building (Averbuch et al., 2005), and bolide impacts (McGhee, 2001; Ellwood et al., 2003).

Temperature variations of surface seawater from 25 °C in the Middle Devonian to 32 °C in the Famennian have been recorded by the oxygen isotopes measured on conodont apatite (Joachimski et al., 2004). Short-term temperature variations have been deduced from the oxygen isotope ratios of both conodont apatite and brachiopod calcite in the Late Givetian and at the F–F boundary (Joachimski et al., 2004; Van Geldern et al., 2006). Enhanced sedimentation and preservation of organic matter under dysoxic to anoxic conditions are commonly concomitant with the biotic crises (e.g. Lower and Upper Kellwasser Horizons in the Late Frasnian; Joachimski and Buggisch, 1993).

High-resolution $\delta^{13}C$ records measured on whole-rock carbonate and brachiopod calcite are now available for the Devonian time interval (Buggisch and Mann, 2004; Buggisch and Joachimski, 2006; Van Geldern et al., 2006) (Fig. 1a). The carbonate $\delta^{13}C$ record shows several short-term excursions with amplitudes of about +3‰ (Buggisch and Joachimski, 2006). These positive $\delta^{13}C$ anomalies, whose durations are around less than 1 Myr to a few Myr, were probably induced by perturbations of the carbon geochemical cycle. The observation that organic matter deposition and black shales events, as well as variations in the oxygen isotope composition of biogenic calcite and apatite are frequently associated with positive $\delta^{13}C$ excursions indicates that short-term perturbations of the carbon cycle were driving pCO_2 and climatic changes (Goddéris and Joachimski, 2004). The $\delta^{13}C$ record shown in Fig. 1a corresponds to the available quantitative time series that recorded environmental

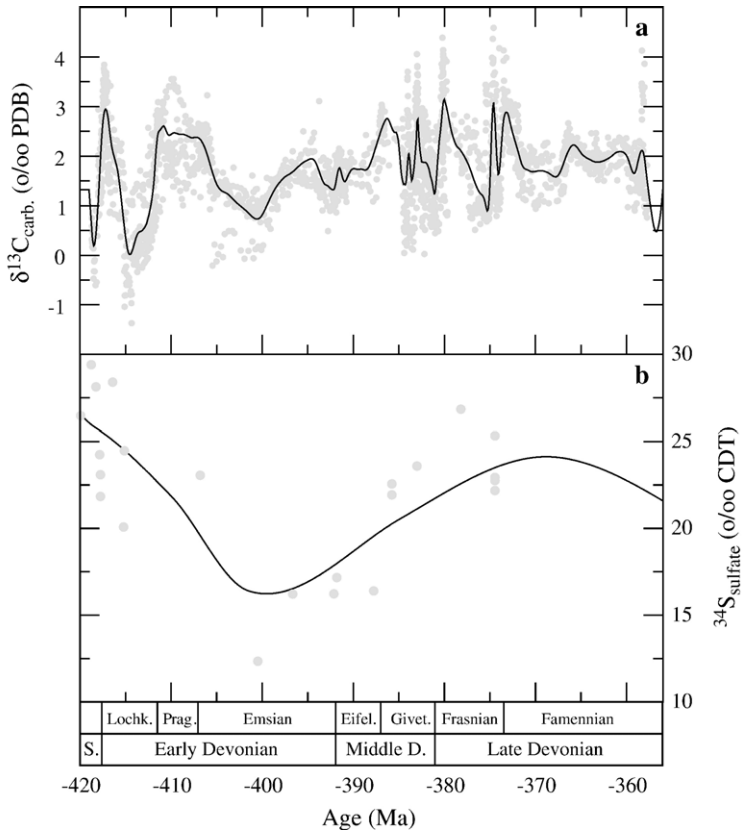

Fig. 1. (a) Carbon isotope composition of Devonian marine carbonates. Grey dots correspond to measured values (Buggisch and Joachimski, 2006; Van Geldern et al., 2006), the black curve is calculated by a 'locfit' local regression. (b) Sulfur isotope composition of Devonian marine sulfate. Grey dots correspond to measured values (Strauss, 1997), the black curve is calculated by a moving average (time step of 5 Myr and window width of 20 Myr).

changes during the Devonian with the highest temporal resolution.

The aims of this study are to calculate the geochemical transfers between the various carbon reservoirs that are documented in the $\delta^{13}C$ record and to reconstruct climatic evolution during the Devonian time interval. The COMBINE model, a numerical model of the carbon, alkalinity, oxygen, sulfur and phosphorus biogeochemical cycles coupled to a 1-D energy-balance climatic model (Goddéris and Joachimski, 2004), computes, among other parameters, the carbon isotope ratios of all dissolved inorganic carbon (DIC) species of each oceanic reservoir. In a direct modeling approach, the calculated $\delta^{13}C$ values are compared to measured carbonate $\delta^{13}C$ and different model parameters and scenarios are tested until agreement is reached (Goddéris and Joachimski, 2004). Such method was already performed for the long-term Phanerozoic fluctuations in marine isotopic ratio (COPSE, Bergman et al., 2004). However, short-term carbon isotope variations are difficult to reproduce. In this study, we used an inverse approach in which the $\delta^{13}C$ of carbonates (Buggisch and Joachimski, 2006) (Fig. 1a) and the $\delta^{34}S$ of marine sulfate (Strauss, 1997) (Fig. 1b) are used as forcing parameters of the carbon geochemical cycle. This is the first inverse approach of a geochemical model that is performed with a 1-D climatic model and applied to study Phanerozoic climate evolution. Previous geochemical models using $\delta^{13}C$ inversion (e.g. GEOCARB III, Berner and Kothavala, 2001; Berner et al., 2000; GEOCARBSULF, Berner, 2006) calculate the mean Earth temperature from a parametric relationship (0-D climatic model). The Earth climate, atmospheric pCO_2 and pO_2 and the composition of seawater are thus computed from the isotopic records at any time.

2. Formulation of the model

The general structure of the COMBINE model is described in Goddéris and Joachimski (2004). COMBINE is an ocean–atmosphere biogeochemical model which is coupled to a 1-D zonal energy-balance climatic model. Compared to the original COMBINE model, some modifications have been made. The ocean geometry has been modified and a sulfur geochemical cycle has been added to the biogeochemical model.

The global ocean is divided into five boxes (Fig. 2). Two epicontinental reservoirs, the surface box ranging from 0 to 100 m depth (surface box) and the deep epicontinental box from 100 to 200 m depth, represent the shallow epicontinental seas. The open ocean is divided in three reservoirs: a photic zone (0–100 m depth), a

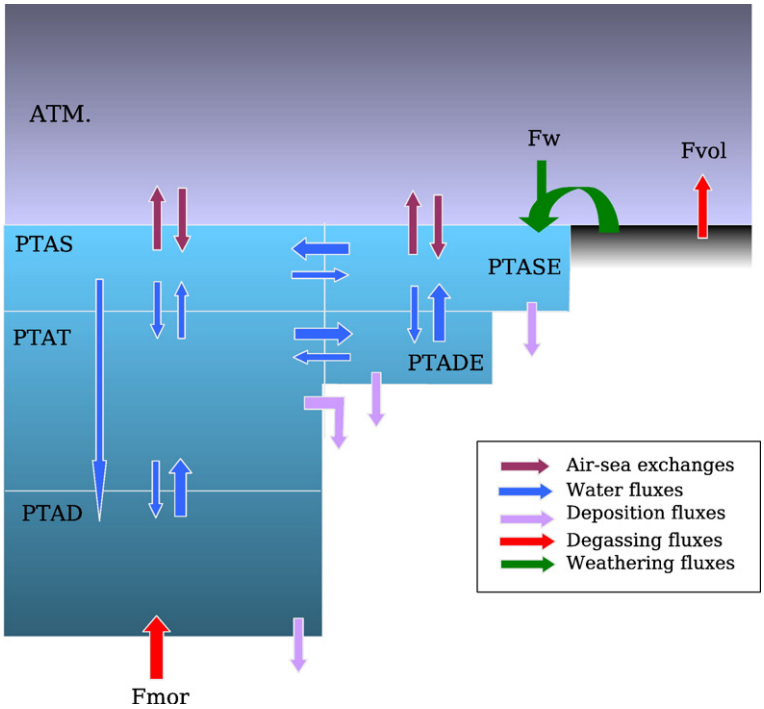

Fig. 2. Schematic view of the COMBINE model. ATM.: atmosphere; PTAS: Panthalassa open ocean surface; PTAT: Panthalassa ocean thermocline; PTAD: Panthalassa ocean deep; PTASE: Panthalassa epicontinental surface; PTADE: Panthalassa epicontinental deep; Fw: Continental weathering flux; Fvol: volcanic degassing flux; Fmor: degassing at mid-ocean ridges.

thermocline (100–1000 m depth) and a deep-sea reservoir (1000 to 5000 m depth). The atmosphere is described by one box connected to the two sea-surface reservoirs. Elements are transferred between fluids and solid Earth's envelopes through geological processes, i.e. continental weathering, sediment deposition, and degassing at mid-ocean ridges and by volcanoes. The energy-balance climatic model, developed by François and Walker (1992), calculates at each time step the mean air temperature in 18 latitude bands as a function of the modeled atmospheric CO_2 content and the latitudinal distribution of continental masses, with a solar luminosity of 98% of the present-day value for the Devonian (Endal and Sofia, 1981). Paleogeographical configuration changes from Late Silurian to Late Devonian and the area and latitudinal repartition of continents are estimated from paleogeographic maps (Scotese and McKerrow, 1990).

2.1. Geochemical cycles

The geochemical cycles for carbon, alkalinity, phosphorus, sulfur and oxygen as well as the ^{13}C and ^{34}S cycles are included in this model. The chemical and isotopic compositions of the atmosphere and each oceanic box are computed at each time step by solving the differential equations that describe their budget.

Carbon inputs in the atmosphere are volcanic degassing and CO_2 degassing at the surface ocean while carbon outputs comprise dissolution of atmospheric CO_2 in sea-surface water and CO_2 consumption by silicate and carbonate weathering. CO_2 consumption by silicate rock weathering is a function of continental runoff, land area, atmospheric CO_2 content and mean zonal air temperature (François and Walker, 1992; Goddéris and François, 1995), and is calculated for each of the 18 latitude bands (Goddéris and Joachimski, 2004):

$$F^{w}(t) = k \times \sum_{j=1}^{18} \left[A_j(t) \times Rf_j(t) \times \exp\left[\frac{-E_a}{R} \left(\frac{1}{T_j} - \frac{1}{288.15} \right) \right] \right] \times f_{CO_2} \times f_e \quad (1)$$

where k is a constant, $A_j(t)$ and $Rf_j(t)$ are respectively the continental area and runoff at any time step in the latitude band j, T_j is the mean air temperature in the latitude band j. R is the gas constant and E_a is the activation energy for the dissolution of silicates. The chemical weathering rate of volcanic rocks is 5 to 10 times higher than the weathering rate of granite and gneiss (Dessert et al., 2001). Different activation energy and k values (respectively, k_{bas} and k_{gra}; $k_{bas}/k_{gra}=10.105$) are considered depending on the lithology: E_a is equal to 42.3 kJ/mol for basalts (Dessert et al., 2001) and 48.7 kJ/ mol for granitic environments (Oliva et al., 2003). We assume a constant ratio between volcanic rocks and granitic lithologies roughly similar to the present-day value, the volcanic surface area representing about 8% of the global silicate area (Dessert et al., 2003). The weathering laws for silicate rocks are calibrated on the compilation of dissolved load data from Dessert et al. (2003) and Oliva et al. (2003). Both studies compile data for monolithological catchments which are experiencing physical erosion as well. For this reason, exporting the weathering laws calibrated for the present day in the distant past implies that the relationship existing between chemical and physical denudation is the same as at present day. This means that Eq. (1) cannot capture the impact of changes in the physical erosion in the past. Since the Devonian tectonic environment might have been rather different compared to the present day one, this hypothesis is probably partially wrong, but conservative in the absence of well constrained data on the physical erosion during the Paleozoic.

The atmospheric CO_2 consumption by carbonate weathering is computed in the same way by using the formulation of François and Walker (1992) and Goddéris and Joachimski (2004):

$$F^{w}_{carb}(t) = k_{carb} \times \sum_{j=1}^{18} \left(A_j(t) \times \sqrt{Rf_j(t)} \right) \times f_{CO_2} \times f_e \quad (2)$$

where k_{carb} is a constant. f_{CO_2} equals $RCO_2^{0.5}$ in the absence of vegetation, where RCO_2 is the atmospheric CO_2 content expressed in present atmospheric level (PAL), and is calculated as follows in the presence of land plants (Berner, 1994):

$$f_{CO_2} = \left(\frac{2RCO_2}{1 + RCO_2} \right)^{0.4}. \quad (3)$$

The factor f_e represents the chemical weathering increase because of the presence of land plants, and is equal to 0.25 for non-vegetated areas and to 0.875 for areas covered by gymnosperms (Berner, 2004).

The content of total dissolved inorganic carbon (DIC), alkalinity, and Ca^{2+} for each oceanic box is computed by solving the differential equations that describe its budget. This part differs from the original COMBINE model (Goddéris and Joachimski, 2004) by the alkalinity budget that takes into account the sulfate fluxes. The inputs are the supply of carbon, alkalinity and calcium to the oceans by weathering of continental rocks, CO_2 degassing at

mid-ocean ridges, atmospheric CO_2 dissolution in surface water and oxidation of organic matter. DIC, alkalinity and Ca^{2+} are exchanged between each oceanic box by water fluxes. Outputs are the CO_2 consumption by photosynthetic activity, carbonate deposition and organic matter burial, and CO_2 degassing at the surface ocean. We assume that the carbonate production by calcareous phytoplankton is negligible during the Paleozoic. Carbonate accumulation occurs only on continental shelves and the related flux is calculated as proportional to $(\Omega_{calcite}-1)^{1.7}$ (Opdyke and Wilkinson, 1988). The calcite saturation ratio, $\Omega_{calcite}$, is determined from the complete carbonate speciation ($[H_2CO_3]$, $[HCO_3^-]$, $[CO_3^{2-}]$, pH, dissolved CO_2) calculated in each oceanic box as a function of salinity, temperature, DIC and alkalinity content. Ocean-surface temperature is calculated as the mean global air temperature estimated by the climatic model, and the deep-sea temperature is set to 276 K.

Particulate organic carbon is produced in the photic zone by biological activity, which is assumed to be proportional to the phosphorus input (Petsch and Berner, 1998). The C:P ratio of the productivity flux is fixed to 117:1 (Anderson and Sarmiento, 1994). The main source of P to the ocean is continental weathering, computed as a function of runoff and vegetation in the same way as carbonate weathering. P output fluxes by P-bearing mineral precipitation (phosphorite, iron hydroxides) are assumed to be proportional to the dissolved phosphorus content of all reservoirs in contact with the seafloor. Recycling of particulate organic carbon and phosphorus occurs within the water column as a function of the dissolved oxygen content. To quantify the burial flux of carbon and phosphorus, a sedimentary model calculates the amount of organic carbon and phosphorus oxidized by oxygen in the uppermost sediment layer and by sulfate reduction deeper in the sediment (François and Walker, 1992; Goddéris and Joachimski, 2004) (see Appendix). The C:P ratio of the buried organic matter increases with the degree of anoxia of bottom waters (Van Cappellen and Ingall, 1996).

An addition to the original COMBINE model is a simple sulfur cycle. The input of sulfur to the ocean occurs in the surface epicontinental reservoir and consists of dissolved sulfate produced by continental weathering of evaporites and pyrite. The sulfur weathering fluxes are difficult to estimate, particularly pyrite weathering since it involves oxidation of rocks, and is thus strongly related to denudation and uplift rates (Petsch et al., 2000). These parameters cannot be estimated for the Paleozoic with a reasonable accuracy. We choose the simple approach of François and Walker (1992) and Kampschulte and Strauss (2004) where both evaporite and pyrite weathering fluxes are assumed to be proportional to the model calculated runoff and to the size of the sedimentary sulfur reservoirs. This is a first-order approach, but pyrite oxidation and evaporite dissolution certainly depend on the amount of available water. Furthermore, this approach is consistent with Petsch et al. (2000), showing that pyrite weathering is not dependent on oxygen content at Phanerozoic levels.

The proportionality constants (Table 1) are fixed so that the present-day sulfur fluxes are reproduced (Petsch and Berner, 1998). Further modeling should account for physical erosion, but this will require an accurate knowledge of tectonic activity in the past, as well as the knowledge of the link between chemical and physical erosion for this type of rocks. The outputs are represented by gypsum and pyrite burial and sulfur uptake during hydrothermal alteration of the oceanic crust. Evaporites are precipitated in epicontinental seas and are buried in the sedimentary sulfate reservoir. The deposition rate of evaporites is assumed to be proportional to the sulfur content of bottom waters (François and Gérard, 1986). Sedimentary pyrite is formed from dissolved seawater sulfate via bacterial sulfate reduction and its burial rate is computed from the seawater sulfate isotope record (see next section). The $\delta^{34}S$ value of degassed sulfur is set equal to the mantle value of 0‰ CDT. The isotopic difference between dissolved seawater sulfate and gypsum sulfate equals +2‰ (Walker, 1986). The fractionation between dissolved seawater sulfate and biogenic pyrite sulfide, estimated from the Devonian seawater surface value of +20‰ (Strauss, 1999) and the pyrite deposit composition of around +10±10‰, leads to an average sulfur isotope fractionation of −30‰.

At the million-year time scale, the oxygen sources are the burial of organic matter and pyrite, and the sinks are the oxidation of reduced sedimentary carbon and pyrite

Table 1
Present-day carbon and sulfur fluxes used for calibration

Flux	Value	Reference
Carbonate weathering F_{cw}	20.6×10^{12} mol/yr	Petsch and Berner (1998)
Continental silicate weathering F_{silw}	11.7×10^{12} mol/yr	Gaillardet et al. (1999)
Continental organic carbon oxidation F_{kerw}	4.1×10^{12} mol/yr	Petsch and Berner (1998)
Continental sulfate weathering F_{Sox}	1.33×10^{12} mol/yr	François and Walker (1992)
Continental sulfide weathering F_{Sred}	0.65×10^{12} mol/yr	François and Walker (1992)

exposed to continental weathering. The sulfur liberated during pyrite weathering is transported to the oceans as sulfate and the crustal carbon as dissolved inorganic carbon. The model does not introduce a dependency of the continental pyrite weathering rate on atmospheric O_2 content, assuming that the rates of weathering are limited by material exposure rather that by O_2 availability (Holland, 1978; Petsch and Berner, 1998). Unlike the original COMBINE model, the oxidation rate of the continental organic matter is calculated from the carbon isotope composition of marine carbonates (see next section). For numerical stability reasons, a flux of O_2 consumption by the oxidation of oceanic rocks has been taken into account and is represented by the oxidation of the fayalite component of silicates to magnetite during hydrothermal alteration of the oceanic crust (Shanks et al., 1981). This O_2 consumption flux is set proportional to the oceanic crust production and to the dissolved oxygen content in the deep oceanic reservoirs, and is calibrated according to the net flux of Fe^{3+} that results from the oxidation of ferrous to ferric iron by seawater (Lécuyer and Ricard, 1999). The concentration of oxygen dissolved in oceanic surface waters is calculated according to Wanninkof (1992) as a function of the temperature, salinity, and partial pressure of O_2 in surface waters, taking into account the diffusion of O_2 at the atmosphere–ocean interface.

Some modifications have been made to the C cycle compared to the Goddéris and Joachimski (2004) COMBINE model. The carbon isotope fractionation that occurs during the formation of organic carbon by photosynthetic activity (ϵ_P) is assumed to have been +19‰, which represents the average of ϵ_P values reconstructed for the Middle and Late Devonian (Kuhn et al., 2001). An average $\delta^{13}C$ value of about −26‰ has been taken for Devonian continental organic matter (Peters-Kottig et al., 2006). The $\delta^{13}C$ value of CO_2 degassed at mid-ocean ridges equals the mantle $\delta^{13}C$ (−5‰; Cartigny et al., 2001) which is assumed to have been constant over most of the Earth's history (Cartigny et al., 1998; Coltice et al., 2004). For calibration reasons, the $\delta^{13}C$ of sub-aerial volcanic CO_2 is set at a constant value of −1‰ (Goddéris and Joachimski, 2004), equal to the isotope composition of subducted carbon into the mantle (Coltice et al., 2004). The carbon isotope composition of each DIC species is calculated for each oceanic reservoir, taking into account the isotope fractionation occurring during CO_2 exchange between ocean and atmosphere (Munhoven, 1997). The carbon isotope fractionation factors for each carbonate species and dissolved CO_2 are calculated as a function of temperature (Mook et al., 1974; Freeman and Hayes, 1992) and the carbon isotope fractionation that occurs during the precipitation of carbonates is assumed to be negligible.

2.2. Forcing parameters of the model

The high-resolution $\delta^{13}C$ record of marine carbonates (Fig. 1a; Buggisch and Joachimski, 2006) and the $\delta^{34}S$ record of marine sulfates (Fig. 1b; Strauss, 1997) are used as the forcing parameters of the carbon and sulfur isotope cycles in an inverse model. The inverse procedure is performed to calculate the magnitude of pyrite burial and organic carbon weathering fluxes that are otherwise difficult to model as a function of climate and atmospheric chemistry.

The pyrite burial flux is calculated from the $\delta^{34}S$ of marine sulfates in a similar way as in Kampschulte and Strauss (2004). In the differential equation that describes the S-isotopic budget of dissolved seawater sulfate in the surface epicontinental box, the $\delta^{34}S$ and $d\delta^{34}S/dt$ values are given by the $\delta^{34}S$ record (Strauss, 1997). The pyrite deposition flux is thus algebraically calculated. Other sulfur fluxes are computed by the model (Section 2.1) at each time step.

We similarly use the carbon isotope composition of marine carbonates as a forcing parameter of the carbon geochemical cycle. Because of the large carbon isotope fractionation that occurs between inorganic carbon and organic matter, excursions in $\delta^{13}C$ of marine carbonates (and consequently in $\delta^{13}C$ of seawater DIC) are likely produced by perturbations of the organic carbon subcycle. However, the weathering rate of sedimentary organic carbon remains poorly known. Oxidation of organic matter has been experimentally studied by Chang and Berner (1999). Kinetics of coal organic matter oxidation by O_2 under water-saturated conditions is fast on a geologic time scale, supporting the assumption that uplift and erosion are the limiting factors for organic carbon weathering, and that atmospheric O_2 content may not affect the oxidation rate of organic matter (Holland, 1984; Petsch and Berner, 1998; Chang and Berner, 1999).

The $\delta^{13}C$ of the epicontinental surface water, $\delta^{13}C_{ES}$, can be calculated by the following differential equation:

$$\begin{aligned} M_{ES}\cdot\frac{d\delta^{13}C_{ES}}{dt} = {} & F_{kerw}\cdot\left(\delta^{13}C_{ker}-\delta^{13}C_{ES}\right) \\ & + F_{ED\rightarrow ES}\cdot\left(\delta^{13}C_{ED}-\delta^{13}C_{ES}\right) \\ & + F_{OS\rightarrow ES}\cdot\left(\delta^{13}C_{OS}-\delta^{13}C_{ES}\right) \\ & - F_{bio}\cdot\left(\delta^{13}C_{H_2CO_3}-\epsilon_P-\delta^{13}C_{ES}\right) \\ & + F_{cw}\cdot\left(\delta^{13}C_{cw}+\delta^{13}C_{atm}-2\delta^{13}C_{ES}\right) \\ & + 2F_{silw}\cdot\left(\delta^{13}C_{atm}-\delta^{13}C_{ES}\right) \\ & + F^{13_C}_{ocean\leftrightarrow ES} \end{aligned} \quad (4)$$

where M_{ES} is the mass of dissolved inorganic carbon in the epicontinental surface box, F_{kerw} is the carbon flux

from continental organic carbon weathering, $F_{OS\rightarrow ES}$ and $F_{ED\rightarrow ES}$ are respectively the DIC mass flux from the surface open ocean and deep epicontinental to the epicontinental surface reservoir, F_{bio} is the flux of carbon uptake by photosynthetic activity, and F_{cw}, $\delta^{13}C_{cw}$ and F_{silw}, $\delta^{13}C_{silw}$ are the carbon fluxes and carbon isotope composition of continental weathering of carbonates, and silicates respectively. $\delta^{13}C_{ker}$ is the carbon isotope composition of the continental organic matter, $\delta^{13}C_{OS}$, $\delta^{13}C_{ED}$, $\delta^{13}C_{H_2CO3}$ and $\delta^{13}C_{atm}$ are the respective carbon isotope compositions of the DIC of the surface open ocean and deep epicontinental DIC reservoir, H_2CO_3 of the surface epicontinental reservoir and atmospheric CO_2. $F^{13c}_{ocean\rightarrow ES}$ is the net exchange of isotopes at the interface of the atmosphere–surface epicontinental reservoir (see Appendix).

The inversion is performed by algebraically calculating F_{kerw} from $\delta^{13}C_{ES}$ and its derivative over time, both obtained from the carbonate $\delta^{13}C$ curve. All other fluxes, carbon concentration and isotopic composition are intrinsically computed by the COMBINE model at each time step. By forcing the rate of pyrite burial and continental organic carbon weathering with the isotope data, the model will calculate atmospheric pCO_2 and climate evolution that is in agreement with the available $\delta^{13}C$ and $\delta^{34}S$ curves. But consequently to the inversion procedure, the origin of the computed variations of these forced fluxes cannot be deduced from the modeling. More details about the model can be found in the Appendix.

2.3. Calibration procedure

The model is calibrated in direct mode and in its present-day configuration (present-day continental configuration and including the formation and deposition of pelagic carbonates) with temperature and runoff calculated under present-day climatic conditions (present-day solar luminosity, 1 PAL atmospheric pCO_2), according to the procedure described in Goddéris and Joachimski (2004). The weathering constants are estimated using the global consumption fluxes of atmospheric CO_2 by the weathering of the different lithologies. k_{carb} is calculated from CO_2 consumption by carbonate weathering (20.7×10^{12} mol/yr; Table 1; Petsch and Berner, 1998). k_{gra} and k_{bas} are estimated from the CO_2 consumption rate derived from basalt weathering of 4.08×10^{12} mol/yr (Dessert et al., 2003), representing between 30 and 35% of the global atmospheric CO_2 consumption by weathering of continental silicates (11.7×10^{12} mol/yr; Table 1; Gaillardet et al., 1999). Calibration of oceanic and sediment numeric modules are performed by adjusting the model constants to obtain DIC, alkalinity, oxygen depth profiles similar to the present-day gradients. Note that for the calibration procedure in direct mode, a flux of continental organic matter weathering corresponding to a present-day O_2 consumption of 4.1×10^{12} mol/yr of O_2 (Table 1; Petsch and Berner, 1998) is required.

The COMBINE model is then run in the Early Devonian configuration with a constant CO_2 degassing rate of 4.5×10^{12} mol/yr (1.25 times the present-day carbon degassing flux estimated to 3.6×10^{12} mol/yr; Gaffin, 1987; Marty and Jambon, 1987; Varekamp et al., 1992; Sano and Williams, 1996) until steady state is reached. The steady-state atmospheric pCO_2 and pO_2 respectively reach 3095 ppmv (11.1 PAL) and 0.113 bar (0.54 PAL) at the Silurian–Devonian boundary. $\delta^{13}C$ of dissolved inorganic carbon in the surface epicontinental seawater stabilizes at +1.3‰. The accumulation rate of carbonates on the epicontinental shelves reaches 13.5×10^{12} mol/yr and the burial rate of organic carbon is 3.8×10^{12} mol/yr.

3. Results of the models

3.1. Reference run

The first simulation (REF) considers changes in the configuration of the continents (i.e. area and latitudinal repartition of continents) during the Devonian. Atmospheric pCO_2, calculated from the inversion of the $\delta^{13}C$ (Fig. 3a) and $\delta^{34}S$ Devonian curves, decreases from a maximum of 3000 ppmv at the Silurian–Devonian boundary to a minimum of 1300 ppmv during the Frasnian (Fig. 3b). Short-term variations in the CO_2 concentration are superimposed on this general trend. The Silurian–Devonian boundary is characterized by a decrease in pCO_2 of 1100 ppmv in 1.5 Myr while the carbonate $\delta^{13}C$ record exhibits a +3‰ positive excursion (Fig. 3a). The long-term decrease in pCO_2 starts in the upper Lochkovian and minimum CO_2 contents of 2000 ppmv are calculated for the Pragian. During the Emsian, atmospheric pCO_2 progressively increases up to 2500 ppmv and subsequently decreases to reach a value of 1500 ppmv at the Eifelian–Givetian boundary. The calculated negative pCO_2 excursion at the Eifelian–Givetian boundary is well correlated with a +1.5‰ excursion in $\delta^{13}C$. Another decrease in pCO_2 is calculated for the Frasnian *P. falsiovalis* conodont Zone and at the Frasnian–Famennian transition, where the calculated pCO_2 gives minimum values around 1300 ppmv. Atmospheric pCO_2 remains around 1600 ppmv during the Famennian (Fig. 3b).

The changes in atmospheric CO_2 concentration are driven by the net carbon balance between the release by oxidation of continental kerogen and the consumption

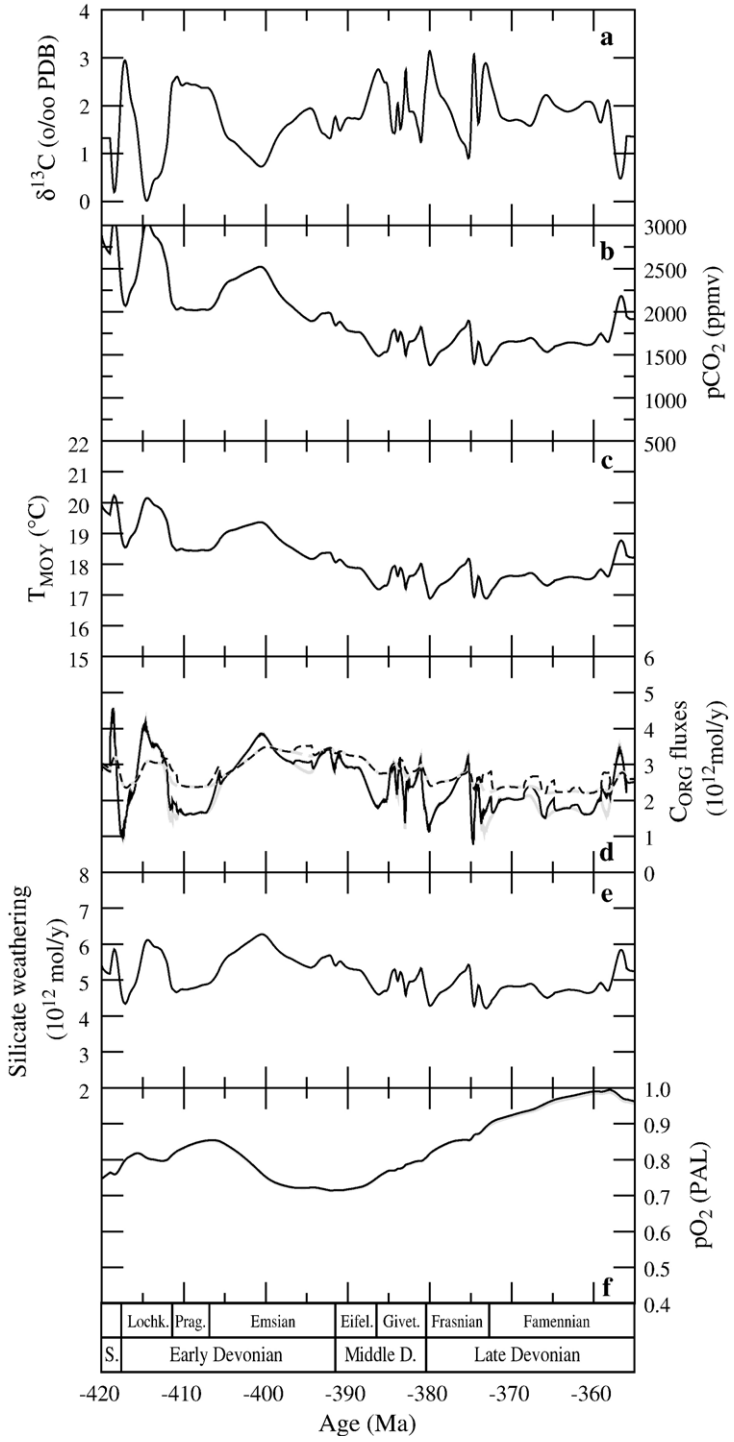

Fig. 3. Results of the REF simulation (grey curves) and of the SWC simulation (black curves). (a) $\delta^{13}C$ of dissolved inorganic carbon within the surface epicontinental reservoir. (b) Atmospheric pCO_2. (c) Mean air temperature at Earth's surface. (d) Organic carbon fluxes; plain line: continental organic carbon oxidation; dashed line: total burial of organic carbon. (e) Global continental silicate weathering. (f) Atmospheric pO_2. (g) Misbalance between organic carbon burial and oxidation of continental organic carbon. (h) Calculated organic carbon content of sediments. (i) Dissolved oxygen concentration; plain line: surface epicontinental reservoir; dashed line: deep epicontinental reservoir. (j) Phosphorus supply to the ocean by continental weathering. (k) Depositional carbonate flux. (l) Phosphate concentration of epicontinental surface reservoir (plain line) and epicontinental deep reservoir (dashed line).

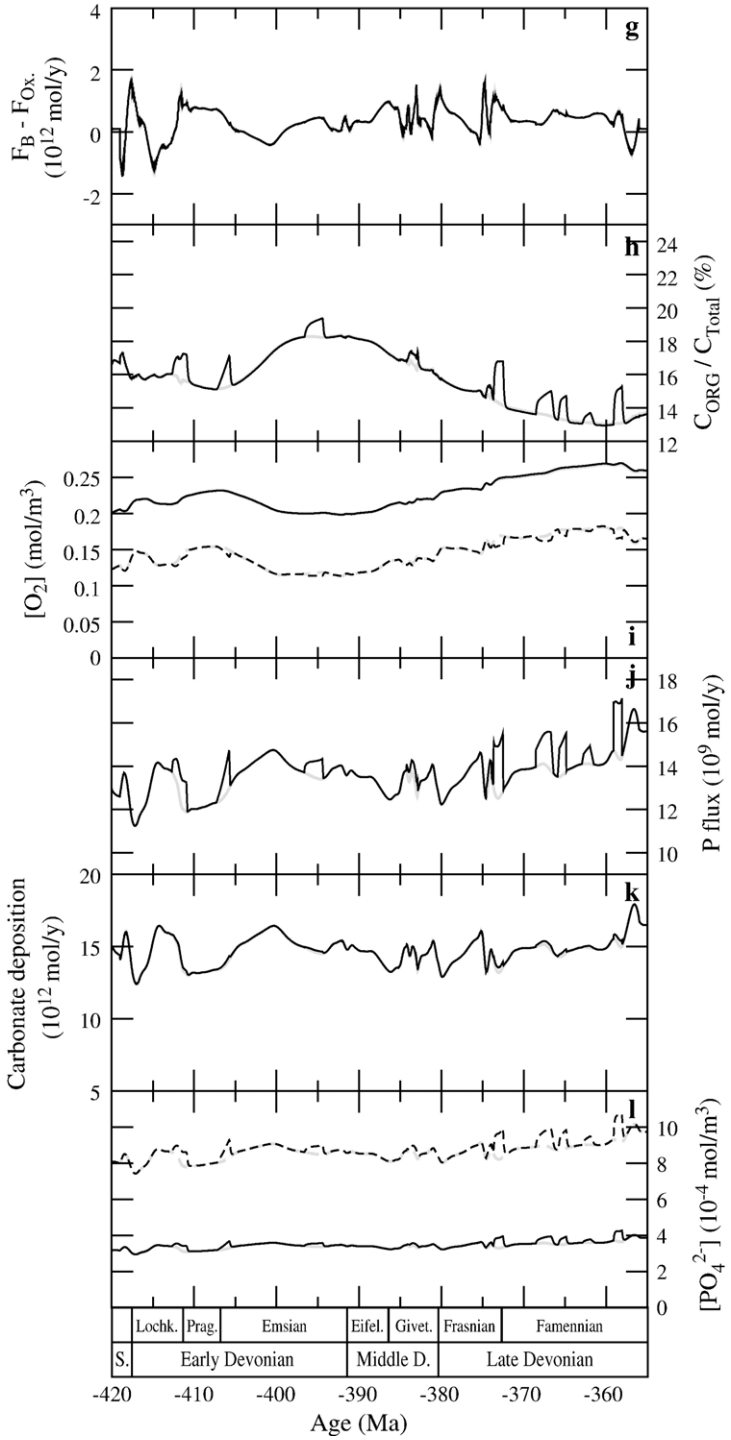

Fig. 3 (*continued*).

by organic matter burial into sediments (Fig. 3d; g). When the carbon isotope composition of epicontinental surface water DIC exhibits a positive excursion, the carbon supply to seawater by kerogen weathering shows minimum values (Fig. 3d) and leads to a pCO_2 decrease (Fig. 3b), partly damped by the silicate weathering negative feedback. Total organic carbon burial mostly varies between 1 and 5×10^{12} mol/yr (Fig. 3d) and

carbonate production ranges between 12 and 17×10^{12} mol/yr (Fig. 3k). The decrease of organic carbon burial, coeval with the positive excursion in carbonate $\delta^{13}C$, is mainly due to a decrease in primary productivity which is triggered by minor phosphorus input (Fig. 3j). The calculated ratio of organic carbon vs. total carbon burial (C_{org}/C_T) reveals a maximum in the Middle Devonian (Fig. 3h). The enhanced preservation of organic matter in the sediments is the result of a decrease of atmospheric pO_2 (Fig. 3f) and dissolved oxygen content in seawater (Fig. 3i).

3.2. Sea-level changes

The REF simulation does not take into account the effect of rapid sea-level variations. Sedimentological records indicate concomitant changes of carbonate $\delta^{13}C$ values, organic carbon contents, and sea-level elevation (Buggisch and Joachimski, 2006). Goddéris and Joachimski (2004) have shown that short-term positive $\delta^{13}C$ excursions and increases in organic carbon deposition can be driven by enhanced riverine phosphorus inputs to the epicontinental ocean reservoir. Enhanced delivery of phosphorus to the ocean can be the result of sea-level changes. Lowering of sea level will increase the continental area and expose carbonate platforms to continental weathering and thus affect the continental weathering fluxes.

The sea-level record of the Devonian (Johnson et al., 1985, 1996) indicates a long-term sea-level rise. The effects of long-term sea-level variations (i.e. continental and oceanic areas, volume of the oceanic reservoirs) are taken into account together with changes in paleogeography. The amplitude of the sea-level rise from the Lower Devonian to the Frasnian–Famennian highstand is not known but was probably more than several tens of meters according to the large flooded area of the North-American craton (Johnson, 1970). For this modelisation and in order to account for the maximum possible effect, we assumed a sea-level rise of 100 m from the Lower Devonian to Frasnian–Famennian boundary, hence calculating amplitudes of second-order sea-level changes of about 5 to 25 m.

These second-order sea-level fluctuations are too rapid to be induced by variations in the volume of the mid-ocean ridge system, and there is no evidence that they are induced by glacio-eustatic changes. Since it is not possible to constrain the causes of these sea-level changes, we model the variations in sea level by artificially deepening or pushing up the deep seafloor at constant water volume (Goddéris and Joachimski, 2004). Consecutive changes in continental area are quantified by the model which uses a hypsometric curve to estimate the volume and horizontal surfaces of the oceanic reservoirs as a function of sea level.

In order to test the maximum effect of short-term sea-level changes on the carbon cycle, we assumed (SWC simulation) that the entire continental area exposed to atmospheric weathering was covered by platform carbonates that were deposited during sea-level highstands. We assumed that carbonates contain P at a C:P ratio of 1000:1 (Froelich et al., 1982). Indeed, the effect of sea-level changes on the weathering fluxes was calculated to be minor if the change in the continental area did not coincide with a change in lithology since decreasing runoff (drier climate) compensated for the larger continental area (Goddéris and Joachimski, 2004). The model estimates the supplementary amount of carbon and phosphorus supplied to the surface epicontinental reservoir as a function of the climate through the dissolution of subaerially exposed platform carbonates.

The main effect of sea-level changes can be observed for the calculated phosphorus fluxes: sea-level falls are responsible for short-term increases of the P weathering flux ranging from around 4 to 20% (Fig. 3j). Consequently, the calculated C_{org}/C_T ratios show prominent positive excursions when compared to the REF scenario (Fig. 3h). High organic carbon contents are computed for the Lochkovian–Pragian boundary interval, at the end of the Emsian, and during the Frasnian and Famennian. The sedimentary organic carbon content is particularly high at the Frasnian–Famennian boundary (Upper Kellwasser event; Fig. 3h).

However, short-term sea-level variations do not significantly affect calculated atmospheric CO_2 concentration (Fig. 3b). The organic carbon burial is increased during sea-level falls (Fig. 3h) as a consequence of enhanced phosphorus supply by rivers (Fig. 3j), increased phosphate content in seawater (Fig. 3l), and slight lowering of dissolved oxygen in the deep oceanic reservoirs (Fig. 3i). Nevertheless, the model response to the external forcing by carbonate $\delta^{13}C$ imposes the difference between continental organic carbon weathering and organic carbon burial. There is thus almost no change in the balance between organic carbon deposition and oxidation (Fig. 3g), and negligible changes in the calculated atmospheric pCO_2 compared to the REF scenario (Fig. 3b). It is also noteworthy that the model calculates the increases of organic carbon burial without deep oceanic anoxia. As already stated by Goddéris and Joachimski (2004), the decline of the oceanic oxygen level is responsible for a limited decrease of the total organic carbon burial in the REF scenario because of a lower biological productivity in the epicontinental

surface reservoir. In contrast, enhanced organic carbon burial seems to be controlled by the supply of phosphorus to the ocean, which rapidly increases during sea-level falls.

3.3. Effect of continental vegetation

The colonization of continental areas by vascular plants during the Devonian might have strongly affected the biogeochemical carbon cycle and Earth's climate (Algeo et al., 1995; Algeo and Scheckler, 1998; Berner, 1998). The colonization of non-vegetated surfaces by gymnosperms, the development of soils and intensification of microbial activity are likely to have caused enhanced weathering of continental surfaces, expressed in the model by increasing the f_e constant from 0.25 to 0.875 in Eqs. (1) and (2). (Berner, 2004). Moreover, enhancement of silicate weathering by pedogenic alteration resulted in a major change in the dependence of chemical weathering on atmospheric CO_2 (f_{CO_2}, Eq. (3)) (Berner, 1994).

Quantifying the vegetation coverage during the Late Paleozoic is a difficult task, and no data on the spreading rate of vascular plants during the Devonian are available. But a tentative scenario can be build.

Before the Middle Devonian, vegetation was restricted to moist areas and habitats that were humid at least during a certain period of the year, since isosporous land plants, like most extant lycopsids and ferns and extant equisetaleans are dependent on water for their reproduction as they release free-swimming sperm cells and the delicate gametophytes are often very vulnerable against desiccation. Given this constraint, it can safely be assumed that the vegetation coverage at that time was less than 10% of the existing land area. Furthermore, early land plants were small and had no or only poorly developed roots (Algeo and Scheckler, 1998). Their influence on soil formation and silicate weathering is expected to have been limited.

Heterospory is an important evolutionary innovation of the Middle Devonian. Heterosporous plants are less dependent from free water because they have no free-living gametophytes and both the megaspores and microspores in which the mega- and microgametophytes develop may be dormant for a certain time. Therefore, they are able to colonize temporarily drier habitats but they still need free water to carry the free-swimming sperm cells to the egg cells of the megagametophyte. Middle Devonian plants were taller and had deeper penetrating rooting systems. The first, still leafless trees attaining a height of up to 8 m (Stein et al., 2007) appeared in the Early Middle Devonian. It is assumed that these forests were widespread in a low south latitude warm temperate zone along the Laurentian and northern European margins of the Acadian mountain belt, as well as in adjacent portions of Gondwana including South America (Stein et al., 2007). We can assume that vegetation coverage reached about 30% of the existing land area.

With the development of seeds in the Late Devonian, plants became fully independent from water for their reproduction, at least for the transfer of the genetic material. Therefore they were able to colonize, previously uninhabited hinterland regions (Mosbrugger, 1990). In the Late Devonian archaeopterids achieved the greatest size with stems of up to 1.5 m in diameter. Arborescence was accompanied by the development of larger root systems responsible for an increase of substrate weathering.

The Late Carboniferous is characterized by a very high production of terrestrial biomass, which is primarily documented by very widespread coal deposits in the paleotropics and subtropics. Although little is known about the vegetation of the extrabasinal regions because most of our information is from coal-forming environments, it is clear that extrabasinal vegetations, adapted to drier conditions must have existed. Leary and Pfefferkorn (1977) described an upland flora from the Early Pennsylvanian of the Illinois Basin. Also palynological data demonstrate the presence of a hinterland vegetation; the genus *Potonieisporites*, which is generally interpreted as conifer prepollen appears as early as the Early Namurian, although the oldest known conifer megafossils have been described from the Westphalian B (Scott and Chaloner, 1983) and conifers did not become really common until the Permian. However, the upper Bolsovian and the Westphalian D is locally characterized by larger amounts of conifer fossils, megafossils (Lyons and

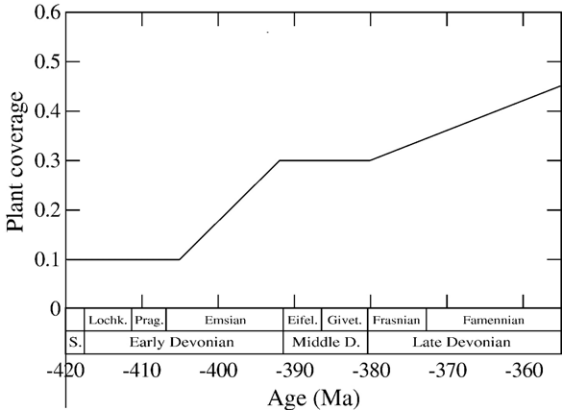

Fig. 4. Vegetation coverage evolution used in the VEG simulation.

Darrah, 1989; Rothwell et al., 1997) and palynological data (Bless et al., 1977).

As a consequence, we assumed a vegetation coverage of about 40–50% for the latest Devonian, considering that the vegetation coverage was total by the end of the Carboniferous (Fig. 4).

We modified the SWC scenario by introducing the consequences of enhanced plant coverage (VEG simulation).

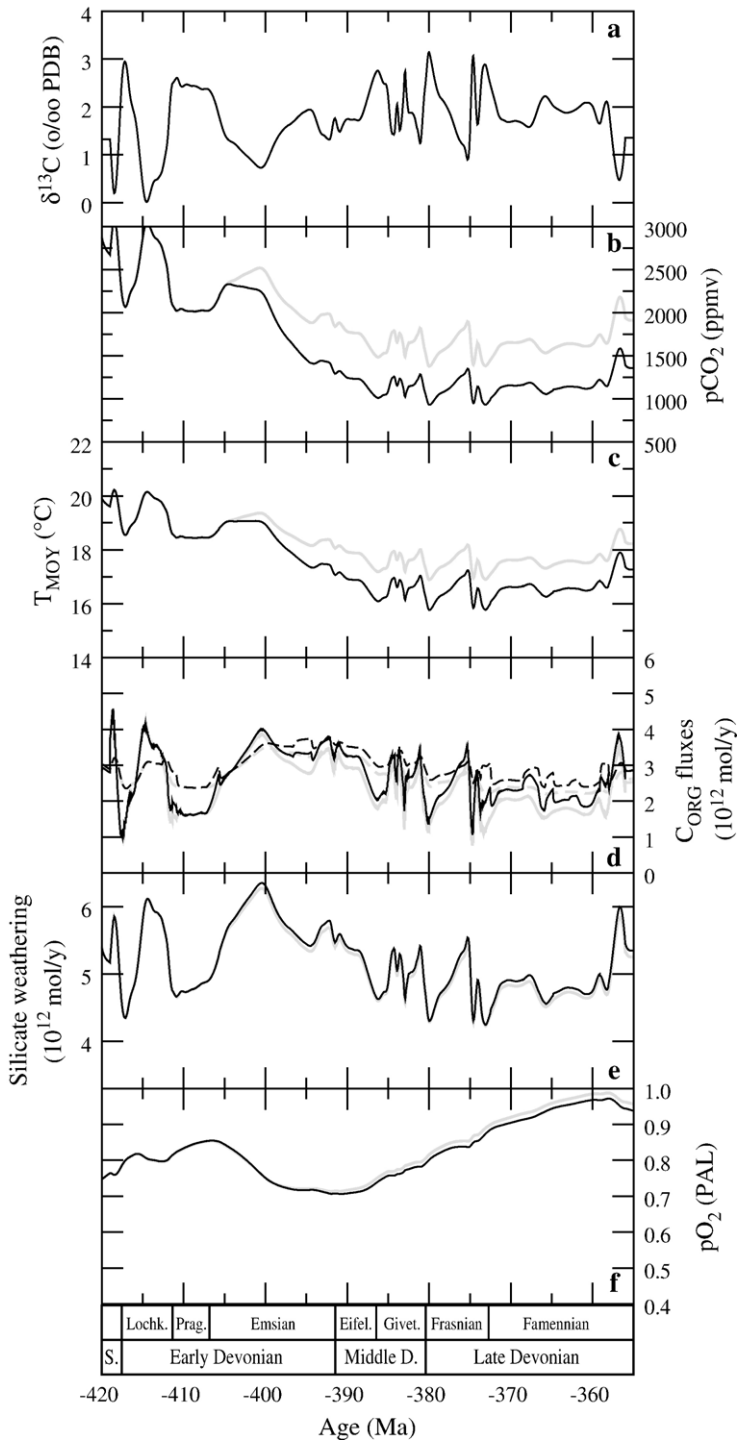

Fig. 5. Results of the VEG simulation (black curves) compared to the REF simulation (grey curves). Same caption as Fig. 3.

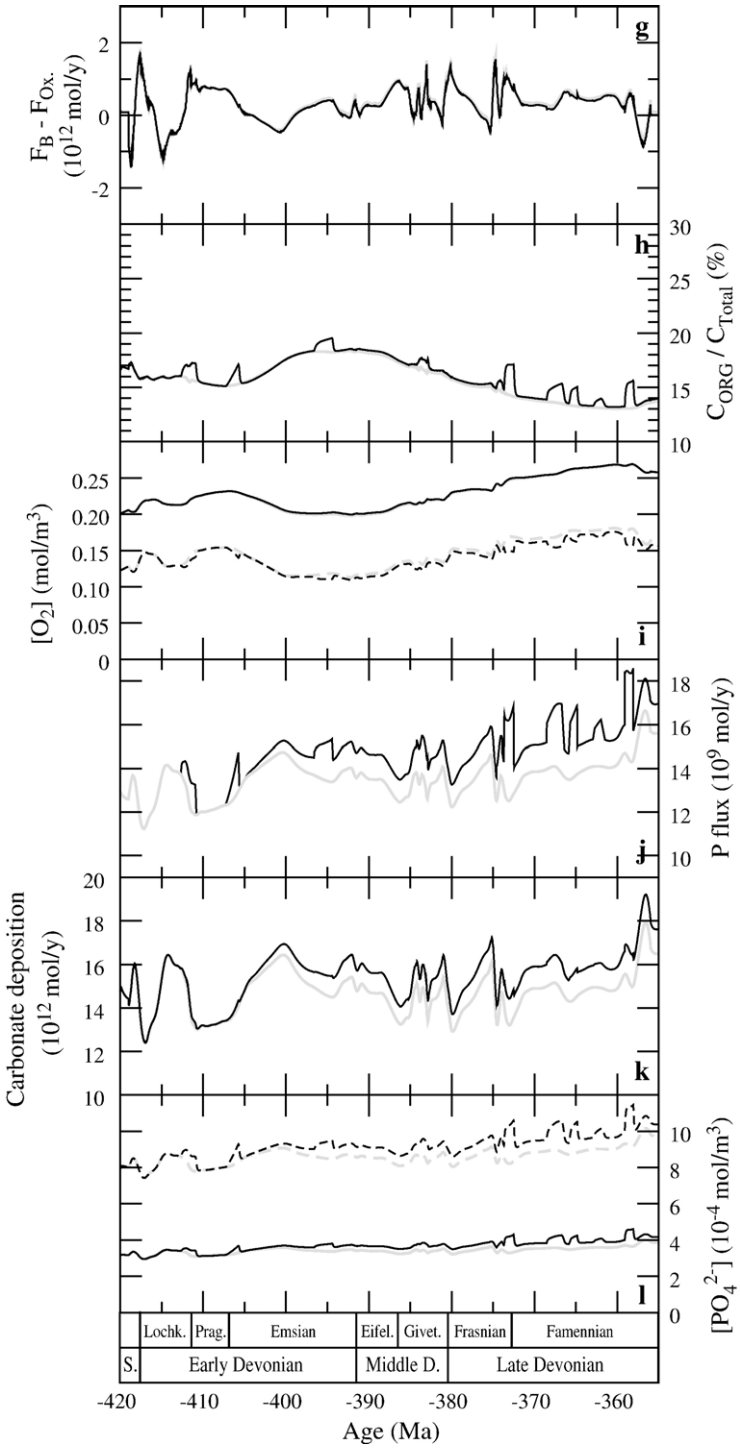

Fig. 5 (*continued*).

Starting from a vegetation that covered 10% of the continental area during the Lochkovian and Pragian, the vegetation coverage increases during the Emsian up to 30%, a value kept constant during the Middle Devonian, and finally, a vegetation coverage of 45% is assumed for the Late Devonian.

Land plant coverage has a major effect on atmospheric pCO_2 evolution (Fig. 5b). The increase of vegetation

coverage at the beginning of the Emsian results in a decrease of pCO_2 from close to 3000 ppmv at the Silurian–Devonian boundary to 1000 ppmv during the Eifelian (Fig. 5b), much lower than the decrease to 1500 ppmv calculated by the REF and SWC simulations. The Middle Devonian maximum in atmospheric pCO_2 of 1250 ppmv occurred at the end of the Givetian and is followed by another decrease with a minimum value of 900 ppmv at the Middle/Late Devonian boundary (Fig. 5b). The atmospheric CO_2 content increases during the Frasnian to 1250 ppmv and decreases again to 900 ppmv at the Frasnian–Famennian boundary. pCO_2 remains stable at around 1100 ppmv until the end of the Famennian (Fig. 5b).

The lower atmospheric CO_2 contents calculated by the VEG scenario are driven by the increase of the organic carbon burial flux resulting from enhanced silicate weatherability and intensified supply of nutrients (P) to the epicontinental surface reservoir (Fig. 5j). The higher dissolved phosphate delivery to the ocean (Fig. 5j) leads to increased oceanic phosphorus content (Fig. 5l) and to higher biological productivity. As a result, sedimentary organic carbon contents increase by a few percent during the Middle and Late Devonian (Fig. 5h). Moreover, the higher organic carbon burial calculated by the VEG scenario (Fig. 5d) is the result of a lower O_2 content in the atmosphere despite a similar long-term pO_2 evolution during the Devonian: pO_2 exhibits a minimum value of 0.70 PAL during the Emsian and increases up to 0.95 PAL at the Devonian–Carboniferous boundary (Fig. 5f). The mean computed atmospheric oxygen levels for the Devonian are thus around 0.8 PAL (16.5%), in agreement with previous low-resolution model estimates of 15 to 20% (Berner, 2001).

The atmospheric pCO_2 records modeled by the REF and VEG scenarios are in good agreement with the available Paleozoic pCO_2 reconstructions from pedogenic carbonates and stomatal indices, despite their range of uncertainties (Royer et al., 2001; Fig. 6). Furthermore, the mean atmospheric CO_2 levels calculated in this study agree with the range of estimates of previous modeling studies (GEOCARB III: Berner and Kothavala, 2001; Fig. 6). However, the general evolution of the atmospheric CO_2 calculated by COMBINE differs significantly from the GEOCARB III estimation. We found that atmospheric CO_2 displays a major decrease from the Middle Emsian up to the Frasnian–Famennian boundary, while GEOCARB III shows a major increase for the same time period. This difference is mainly related to the updated $\delta^{13}C$ curve used to perform the inversion. Furthermore, using carbonate $\delta^{13}C$ data with high temporal resolution as forcing parameter of the COMBINE model allows to calculate short-term variations of atmospheric pCO_2 with a time resolution of 0.1 Ma, much lower than time resolution of the GEOCARB model (Berner, 1994; Berner and Kothavala, 2001). Such temporal resolution cannot be reached by GEOCARB-like models, since these models are steady-state models, and their temporal resolution cannot be shorter than several times the residence time of carbon in the ocean–atmosphere system (several times 200 000 yr: François and Goddéris, 1998). COMBINE fully solves the out-of-steady-state evolution of the carbon cycle, including the diffusion process at the ocean–atmosphere interface and the mixing between oceanic boxes, allowing an improvement in temporal resolution of up to several thousand years.

Finally, our simulations do not account for the possible increase in terrestrial organic carbon burial, linked to the rise of continental vegetation. This flux has been large during the Permo-Carboniferous (Berner, 2004). For instance, coal burial reaches 53×10^{15} mol/myr C during the Carboniferous. However, despite the Devonian terrestrialization process, the coal burial was very low at that time (1×10^{15} mol/myr C). Furthermore, the rise in seawater $\delta^{13}C$, often interpreted as the result of an efficient terrestrial carbon burial, starts at the Devonian–Carboniferous boundary (Veizer et al., 1999). The reason for this low Devonian burial is not known. This may be linked either to the nature of the Devonian land plants, but also to the environment of preservation. Although lignin was present in land plant tissues since the Early Devonian (Friedman and Cook, 2000; Boyce et al., 2003), it was not abundant until the rise of large trees during the Middle Devonian (Stein et al., 2007). However, first forests only appear during the latest stage of the Devonian (Famennian)

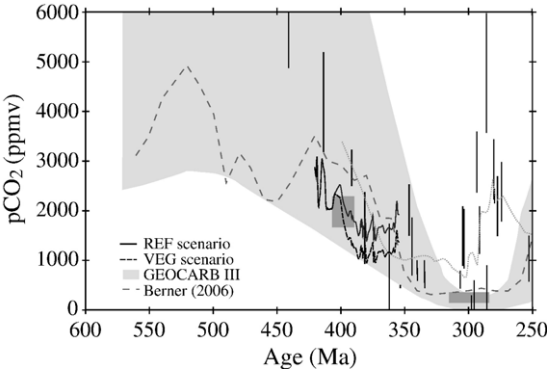

Fig. 6. Comparison of REF and VEG model predictions of atmospheric pCO_2 over the Devonian with pCO_2 estimates from pedogenic carbonate (grey vertical lines; grey dotted line: five-point running average of the mean pCO_2 of every estimate) and stomatal indices (grey filled boxes) (Royer et al., 2001), and with atmospheric pCO_2 calculated by GEOCARB III (Berner and Kothavala, 2001) and GEOCARBSULF (Berner, 2006) over the Paleozoic. The grey envelope represents error estimates in GEOCARB III model (Berner and Kothavala, 2001).

(Scott and Glasspool, 2006), allowing the onset of an abundant litter, itself favouring the burial of terrestrial organic matter. But this was after the Devonian. Furthermore, low sea-level stand during the Permo-Carboniferous may have promoted the extension of coastal lowlands, possibly covered by extensive swamps, allowing massive terrestrial carbon preservation (Berner, 2004), while sea level was higher during the Devonian (Miller et al., 2005).

3.4. Temperature changes during the Devonian

Mean Earth-surface temperature calculated by the SWC scenario (and REF scenario) decreases from 20 °C at the Silurian–Devonian boundary down to 17 °C in the Middle Devonian, and increases up to about 18 °C during the Late Devonian (Fig. 3c). Short-term global temperature variations whose amplitude is around 2 °C are calculated for the Silurian–Devonian and Lochkovian–Pragian boundary intervals. Significant short-term temperature drops are computed for the Early Frasnian and at the Frasnian–Famennian boundary, coincident with the Kellwasser events (Fig. 3c).

The temperature range of 27 to 30 °C calculated by the model for intertropical zones during Early Devonian (Fig. 7) is in agreement with temperatures calculated from oxygen isotopes of conodont apatite (Breisig et al., unpubl. data). $\delta^{18}O$ values of Middle Devonian conodonts (Joachimski et al., 2004) indicate relatively cool surface-water temperatures around 20 to 22 °C, in disagreement with temperatures calculated by the SWC model ranging from 25 to 28 °C (Fig. 7). The SWC model indicates Late Devonian temperatures of 26–29 °C, similar to the temperature deduced from the oxygen isotope composition of conodonts (Joachimski et al., 2004).

The decrease in atmospheric pCO_2 calculated by the VEG scenario leads to calculate lower temperatures for the Middle Devonian (Fig. 5c), as a consequence of enhanced continental weathering and higher organic carbon burial driven by land plant colonization of the continents. The VEG model calculates a long-term decrease of low-latitude temperatures from 26–29 °C at the beginning of the Emsian to 24–26 °C at the end of the Eifelian and at the Givetian–Frasnian boundary (Fig. 7), in good agreement with the temperatures deduced from the oxygen isotope composition of brachiopod shell calcite (Van Geldern et al., 2006), but significantly higher than the temperatures calculated from $\delta^{18}O$ of conodonts. Temperature of 24–27 °C is computed for the Late Devonian (Fig. 7), subsequent to two short-term cooling events at the

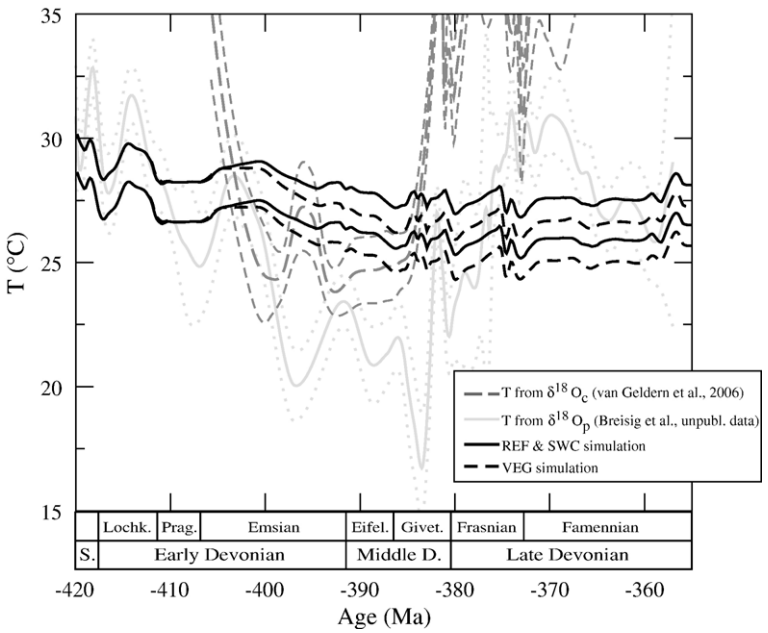

Fig. 7. Calculated evolution of equatorial temperatures during the Devonian. Gray curves correspond to temperatures calculated from the oxygen isotope composition of conodont apatite, considering a $\delta^{18}O$ value of Devonian seawater of −1‰ V-SMOW. The black, plain curves represent the temperature range computed by the REF and SWC simulations, while the dashed curves show the temperature range computed by the VEG scenario. Upper line and lower line represent modeled temperatures for the 0 to 10 and 10 to 20 degree latitude bands, respectively.

Givetian–Frasnian and at the end of the Frasnian whose amplitudes range from 1 to 2 °C (Fig. 7). These cooling pulses correspond well to the *falsiovalis* and Kellwasser events. Modeled ocean temperatures during Late Devonian are difficult to compare to those deduced from the oxygen isotope composition of brachiopod calcite because the low $\delta^{18}O$ values of biogenic carbonates imply surface-water temperatures higher than 33 °C, and sometimes higher than 38 °C (Van Geldern et al., 2006), a value considered lethal for higher marine life (Brock, 1985).

4. Conclusions

The atmospheric pCO_2 and pO_2 contents calculated from the inversion of Late Paleozoic carbon and sulfur isotope records agree relatively well with published long-term reconstructions of these variables (Royer et al., 2001; Berner, 2001). Atmospheric pCO_2 and pO_2 at the end of the Silurian are calculated to have been 3000 ppmv and 0.75 PAL, respectively. During the Devonian, pCO_2 decreases to contents around 1000 ppmv. Based on an updated carbonate $\delta^{13}C$ curve, the inversion modeling provides access to short-term variations of atmosphere and seawater compositions with a much lower time resolution than time resolution of previous models. Short-term variations in atmospheric pCO_2 to 2000 ppmv are calculated for the Silurian–Devonian transition and the Pragian. Lowering of atmospheric CO_2 contents to 900–1000 ppmv is predicted for the Eifelian–Givetian, Givetian–Frasnian and Frasnian–Famennian transitional intervals. These changes in pCO_2 coincide with the occurrences of grey or black shales in the Lochkovian, Eifelian, and Frasnian. In addition, short-term increases of the calculated organic carbon burial rate correspond to the grey and black shale events. The agreement between the sedimentary record and the modeled fluxes is relatively good if rapid sea-level fluctuations are assumed to have been responsible for major changes of the continental phosphorus (or nutrients since P is the only nutrient modeled in this study) supply to the oceans, as already proposed by Goddéris and Joachimski (2004). Most important, the production and preservation of large amount of organic matter in sediments requires enhanced biological productivity, which cannot be sustained in case of anoxia (Goddéris and Joachimski, 2004). It is noteworthy that positive $\delta^{13}C$ excursion will be the result of increased organic carbon burial rates only if the oxidation of continental organic carbon remains constant which generally cannot be assumed since climatic changes are expected to induce a change in continental runoff.

Modeled low-latitude temperatures are compared to paleotemperatures derived from oxygen isotopes of conodont apatite (Joachimski et al., 2004) and brachiopod calcite (Van Geldern et al., 2006). Modeled Early and Late Devonian temperatures range from 27 to 30 °C and 25 to 28 °C, respectively, and are in good agreement with temperatures calculated from the oxygen isotope composition of conodonts and brachiopod calcite. Nevertheless, detailed vegetation data are used to propose a scenario of rapid colonization of continents by land plants during the Middle Devonian, increasing chemical weathering and CO_2 consumption, to account for cooling of surface water down to 25 °C, as suggested by the $\delta^{18}O$ values of conodont apatite (Joachimski et al., 2004). Minimum atmospheric CO_2 concentrations of around 900 ppmv are calculated at the Eifelian–Givetian, Givetian–Frasnian and Frasnian–Famennian transitional intervals. Whatever scenario is considered, short-term cooling events of tropical surface waters of 2 °C are reconstructed for the Silurian–Devonian transition, at the end of the Pragian, and at the Givetian–Frasnian and Frasnian–Famennian transitions. Such temperature variations are in agreement with the temperature changes calculated by Goddéris and Joachimski (2004) across the Frasnian–Famennian boundary.

Acknowledgments

This work was financially supported by the Deutsche Forschungsgemeinschaft and is a contribution to the DFG priority program SPP 1054. Part of the funding was also provided by the CNRS ECLIPSE program. We thank H. Kerp (University of Muenster, Germany) and Brigitte Meyer-Berthaud (CIRAD, Montpellier) for fruitful discussions regarding the land plant colonization during the Devonian. R.A. Berner, an anonymous reviewer and the editor B. Bourdon are greatly acknowledged for improving the quality of the manuscript.

Appendix A

The equation describing the temporal evolution of the concentration Q_i^k of a given species k in the oceanic reservoir i is described by

$$\frac{d\left(V_i \cdot Q_i^k\right)}{dt} = R_i^k + F_{\mathrm{atm}-i}^k + \sum_{j \neq i} \left(F_{ji} \cdot Q_j^k - F_{ij} \cdot Q_i^k\right). \quad (5)$$

V_i is the total water volume of reservoir i, R_i^k is the term accounting for the creation or destruction of the species k

within the reservoir i, $F^k_{\mathrm{atm}-i}$ accounts for the gas exchange between the atmosphere and reservoir i (this term equals zero if the reservoir i is not in contact with the atmosphere, and is positive from the atmosphere to the sea), and the sum represents the mixing term between the various oceanic reservoir through transport (F_{ij} is the water flux from reservoir i to reservoir j). The R^k_i include the biological productivity, the carbonate precipitation, the dissolution of either POC or PIC in the water column, the degassing at mid-oceanic ridges, the uptake of oxygen the oxidation of fayalite component of the silicates during hydrothermal alteration, the discharge of continental runoff. A set of equations is written for DIC, alkalinity, calcium, dissolved oxygen, dissolved PO_4^{2-}, dissolved Sr, PIC, POC, POP, SO_4^{2-}. Once the DIC and alkalinity budgets solved, the pH of seawater is calculated at each time step, together with all dissolved inorganic carbon species through carbonate speciation.

The budget equation for an atmospheric species (namely O_2 and CO_2) is written as:

$$\frac{d\left(V_{\mathrm{atm}}\cdot Q^k_{\mathrm{atm}}\right)}{dt} = R^k_i + \sum_{j=\mathrm{surf}}\left(-F^k_{\mathrm{atm}-j}\right) \tag{6}$$

where the sum extends to the surface oceanic reservoirs (open ocean and epicontinental sea in this case). R^k_i now stands for the consumption or release of the atmospheric species k through geological processes (continental weathering or CO_2 degassing by aerial volcanic activity for instance). Continental weathering fluxes of carbon are detailed in the main text. Atmospheric gas diffusion at the ocean–atmosphere interface is calculated as a function of the gradient of the partial pressure between air and seawater:

$$F^k_{\mathrm{atm}-i} = K_0\cdot\left(P^k_{\mathrm{atm}} - P^k_i\right)\cdot \mathrm{area}_i \tag{7}$$

where K_0 is a constant [K_0=16.016 mol/(yr PAL m^2) for CO_2, and K_0=518.28 mol/(yr PAL m^2) for O_2]. P stands for the partial pressure of the considered gas. P^k_{atm} is directly inferred from:

$$P^k_{\mathrm{atm}} = \frac{V_{\mathrm{atm}}\cdot Q^k_{\mathrm{atm}}}{V_{\mathrm{atm}}\cdot Q^{k,O}_{\mathrm{atm}}} \tag{8}$$

where $V_{\mathrm{atm}}\cdot {Q_{\mathrm{atm}}}^{k,O}$ is the present total content of the atmosphere in species k. P^k_i is estimated through the Henry laws, relating $H_2CO_3^*$ to dissolved PCO_2, and dissolved O_2 to dissolved PO_2. Henry constants $\aleph$ in mol/(l atm) for a given surface reservoir are assumed to be dependent on temperature T_i in K, and salinity S_i in ‰:

$$\ln\left(\aleph^i_{\mathrm{CO_2}}\right) = -58.0931 + \frac{9050.69}{T_i} + 22.294\ \ln\left(\frac{T_i}{10^2}\right) + S_i\left(0.027766 - 0.025888\frac{T_i}{10^2} + 0.0050578\frac{T_i^2}{10^3}\right) \tag{9}$$

$$\ln\left(\aleph^i_{\mathrm{O_2}}\right) = -47.6817 + \frac{8580.79}{T_i} + 23.8439\ \ln\left(\frac{T_i}{10^2}\right) + S_i\left[-0.034892 + \frac{T_i}{10^2}\left(-0.0019387\frac{T_i}{10^2} + 0.015568\right)\right]. \tag{10}$$

Biological productivity F_{bio} in mol/yr of PO_4^{2-} in the photic zone is made dependent on the input of phosphorus through continental upwelling (in the open ocean), and through upwelling and continental weathering (F_{pw}) (in the epicontinental sea):

$$F^{i=\mathrm{surf}}_{\mathrm{bio}} = \rho_i\left(F_{ji}\cdot \mathrm{PO}^{2-}_{4,j} + F_{\mathrm{pw}}\right) \tag{11}$$

where $PO_{4,j}$ is the PO_4^{2-} concentration in the reservoir j. The F_{pw} appears only if the reservoir i is the surface epicontinental sea. ρ_i is an efficiency parameter, cutting down productivity if dissolved CO_2 partial pressure falls below 60 ppmv, to avoid negative carbon content driven by too high productivity in case of very low CO_2 levels. This limit is never reached in the present simulations. Carbon productivity is calculated by multiplying $F^{i=\mathrm{surf}}_{\mathrm{bio}}$ by the redfield ratio of 117.

During this photosynthetic process, O_2 is released with a C/O_2 ratio of 1. Oxic recycling F^i_{recycle}, consuming O_2 and POC and releasing DIC in the thermocline and deep-sea reservoirs, is calculated as follows:

$$F^i_{\mathrm{recycle}} = \left(1. - r^i_{\mathrm{oxyd}}\right)\cdot f_{\mathrm{sink}}\cdot \mathrm{POC}_{\mathrm{above}} \tag{12}$$

where f_{sink} is an adjustable parameter constraining the sink rate of organic matter, $\mathrm{POC}_{\mathrm{above}}$ is the POC concentration in the reservoir overlying the thermocline or deep reservoir i. r^i_{oxyd} is set to 1 if the dissolved O_2 concentration is above 0.2 mol/m_3 (all POC is recycled), and depends linearly on dissolved O_2 content of the reservoir itself. It reaches 0 when O_2 concentration goes down to zero. In all simulation, dissolved oxygen concentration below the surface reservoir is always below 0.2 mol/m^3, and above 0.

When organic matter reaches the seafloor (either in deep-sea environment, and on shelves), it enters a simplistic sedimentary model that calculates the amount of organic matter being finally stored in the sediments. Oxic recycling within a sedimentary mixed layer is

calculated. Assuming that this recycling is a linear function of the O_2 level and of the concentration in organic carbon in the mixed layer, the oxic recycling in the sediment below the deep oceanic reservoir i (either in open ocean environment or on the shelf) can be written as:

$$\int_0^{h_{\mathrm{ml}}} \beta \cdot \mathrm{O}_2^i(x) \cdot \left[C_{\mathrm{org}}^i\right](x) \cdot dx = F_{\mathrm{org}}^{\mathrm{in},i} - \left[C_{\mathrm{org}}\right]^i(h_{\mathrm{ml}}) \cdot w_{\mathrm{s}} \tag{13}$$

where $[C_{\mathrm{org}}^i](x)$ if the organic concentration at depth x inside the mixed layer, $[C_{\mathrm{org}}^i](h_{\mathrm{ml}})$ is the same at the basis of the mixed layer, below the oceanic reservoir i. β is a kinetic parameter (set to 10^{-1} through calibration), h_{ml} is the thickness of the mixed layer (fixed at 20 cm). w_{s} is the sedimentation rate of the sediment, set to a constant 1 mm/year. $\mathrm{O}_2^i(x)$ is the dissolved oxygen concentration at depth x in the mixed layer. $F_{\mathrm{org}}^{\mathrm{in},i}$ is the flux of organic carbon reaching the sediment per m^2 of seafloor surface, depending on the above bio-productivity and recycling in the above reservoirs. Assuming efficient bioturbation, dissolved O_2 level and $[C_{\mathrm{org}}]$ concentration can be considered constant as a function of depth in the sedimentary mixed layer. The integral can thus be easily solved:

$$\left[C_{\mathrm{org}}^i\right](h_{\mathrm{ml}}) = \frac{F_{\mathrm{org}}^{\mathrm{in},i}}{w_{\mathrm{s}} + \beta \cdot h_{\mathrm{ml}} \cdot \mathrm{O}_2^i}. \tag{14}$$

Further oxidation by sulfate reduction occurs below the mixed layer, but this term is assumed to be constant, independently from the model variables.

Oxidation of continental sulfur and dissolution of continental evaporites is assumed to be proportional to continental runoff. Deposition of sedimentary evaporites in epicontinental area is calculated proportional to the modeled epicontinental surface SO_4^{2-} content. Finally, total burial of sedimentary pyrite F_{pyr}^b is estimated based on the inversion of the sulfur isotopic budget. For the sake of simplicity, the burial is assumed to occur on shelves, below the surface epicontinental reservoir:

$$\begin{aligned}\epsilon_{\mathrm{pyr}} \cdot F_{\mathrm{pyr}}^b = & -Q_i^{\mathrm{SO_4}} \cdot V_i \cdot \frac{d\delta^{34}\mathrm{S}}{dt} \\ & + \sum_{j \neq i} \left[F_{ij} \cdot Q_j^{\mathrm{SO_4}} \cdot \left(\delta^{34}\mathrm{S}_j - \delta^{34}\mathrm{S}_i\right)\right] \\ & + F_{\mathrm{pyr}}^w \cdot \left(\delta^{34}\mathrm{S}_{\mathrm{red}} - \delta^{34}\mathrm{S}_i\right) \\ & + F_{\mathrm{evap}}^w \cdot \left(\delta^{34}\mathrm{S}_{\mathrm{evap}} - \delta^{34}\mathrm{S}_i\right) - F_{\mathrm{evap}}^b \cdot \epsilon_{\mathrm{evap}}\end{aligned} \tag{15}$$

where $Q_i^{\mathrm{SO_4}}$ is the sulfate concentration in the epicontinental reservoir i, V^i is the water volume of the reservoir i, $\frac{d\delta^{34}\mathrm{S}}{dt}$ is the time derivative of the measured isotopic signal, $Q_j^{\mathrm{SO_4}}$ is the sulfate concentration in any oceanic reservoir in contact with the epicontinental reservoir, $\delta^{34}\mathrm{S}_j$ its $\delta^{34}\mathrm{S}$ value. $\delta^{34}\mathrm{S}_i$ is the measured $\delta^{34}\mathrm{S}$. F_{pyr}^w and F_{evap}^w are respectively the continental pyrite and evaporite weathering, with their respective $\delta^{34}\mathrm{S}$ ($\delta^{34}\mathrm{S}_{\mathrm{red}}$ and $\delta^{34}\mathrm{S}_{\mathrm{evap}}$). Finally, isotopic fractionation occurring during pyrite burial ϵ_{pyr} and evaporite deposition ϵ_{evap} are set to respectively −30‰ and +2‰.

The isotopic carbon budget is calculated for each reservoirs. ^{13}C exchange fluxes between the atmosphere and the surface ocean boxes are modeled as:

1) flux from the atmosphere to the ocean:

$$\begin{aligned}& f_{\mathrm{atm-oc}}^{13_C} \\ & = \sum_{j=\mathrm{surf}} K_0 \cdot \left[\phi_{as} \cdot \mathrm{PCO}_{2,\mathrm{atm}} - \left(\delta^{13}\mathrm{C}_j - \delta^{13}\mathrm{C}_{\mathrm{atm}} + \phi_{sa}\right) \cdot \mathrm{PCO}_{2,j}\right] \cdot \mathrm{area}_j\end{aligned} \tag{16}$$

2) flux from the ocean to the atmosphere:

$$\begin{aligned}& f_{\mathrm{oc-atm}}^{13_C} \\ & = \sum_{j=\mathrm{surf}} K_0 \cdot \left[\left(\delta^{13}\mathrm{C}_{\mathrm{atm}} - \delta^{13}\mathrm{C}_j + \phi_{as}\right) \cdot \mathrm{PCO}_{2,\mathrm{atm}} - \phi_{sa} \cdot \mathrm{PCO}_{2,j}\right] \cdot \mathrm{area}_j\end{aligned} \tag{17}$$

where the sum extends over all the oceanic and epicontinental surface reservoirs. area_j is the area of those reservoirs, $\mathrm{PCO}_{2,\mathrm{atm}}$ and $\mathrm{PCO}_{2,j}$ are respectively the atmospheric and dissolved CO_2 partial pressures. $\delta^{13}\mathrm{C}_{\mathrm{atm}}$ and $\delta^{13}\mathrm{C}_j$ are the $\delta^{13}\mathrm{C}$ of the atmosphere and dissolved inorganic carbon. ϕ_{as} and ϕ_{sa} are mathematically related to the one-way fractionation factor and are respectively equal to −0.002 and −0.010.

References

Algeo, T.J., Scheckler, S.E., 1998. Terrestrial–marine teleconnections in the Devonian: links between the evolution of land plants, weathering processes, and marine anoxic events. Philos. Trans. R. Soc. Lond., B 353, 113–130.

Algeo, T.J., Berner, R.A., Maynard, J.B., Scheckler, S.E., 1995. Late Devonian anoxic events and biotic crises: 'rooted' in the evolution of vascular land plants? GSA Today 5, 63–66.

Anderson, L.A., Sarmiento, J.L., 1994. Redfield ratio of remineralization determined by nutrient data analysis. Glob. Biogeochem. Cycles 8, 65–80.

Averbuch, O., Tribovilard, N., Devleeschouwer, X., Riquier, L., Mistiaen, B., van Vliet-Lanoe, B., 2005. Mountain building-enhanced continental weathering and organic carbon burial as major causes for climatic cooling at the Frasnian–Famennian boundary (ca 376 Ma BP). Terra Nova 17, 25–34.

Bergman, N.M., Lenton, T.M., Watson, A.J., 2004. COPSE: a new model of biogeochemical cycling over Phanerozoic time. Am. J. Sci. 304, 397–437.

Berner, R.A., 1994. GEOCARB II: a revised model for atmospheric CO_2 over Phanerozoic time. Am. J. Sci. 294, 56–91.

Berner, R.A., 1998. The carbon cycle and CO_2 over Phanerozoic time: the role of land plants. Philos. Trans. R. Soc. Lond., B 353, 75–82.

Berner, R.A., 2001. Modelling atmospheric oxygen over Phanerozoic times. Geochim. Cosmochim. Acta 65, 685–694.

Berner, R.A., 2004. The Phanerozoic Carbon Cycle. Oxford University Press, New York. 150 pp.

Berner, R.A., 2006. GEOCARBSULF: a combined model for Phanerozoic atmospheric O_2 and CO_2. Geochim. Cosmochim. Acta 70, 5653–5664.

Berner, R.A., Kothavala, Z., 2001. Geocarb III: a revised model of atmospheric CO_2 over Phanerozoic time. Am. J. Sci. 301, 182–204.

Berner, R.A., Petsch, S.T., Lake, J.A., Beerling, D.J., Popp, B.N., Lane, R.S., Laws, E.A., Westley, M.B., Cassar, N., Woodward, F.I., Quick, W.P., 2000. Isotopic fractionation and atmospheric oxygen: implications for Phanerozoic O_2. Science 287, 1630–1633.

Bless, M.J.M., Loboziak, S., Streel, M., 1977. An Upper Westphalian 'Hinterland' microflora from the Haaksbergen I borehole. Netherlands. Meded. - Rijks Geol. Dienst 285, 135–149.

Boyce, C.K., Cody, G.D., Fogel, M.L., Hazen, R.M., Alexander, C.M.D., Knoll, A.H., 2003. Chemical evidence for cell wall lignification and the evolution of tracheids in Early Devonian plants. Int. J. Plant Sci. 164, 691–702.

Brock, T.D., 1985. Life at high temperatures. Science 230, 132–138.

Buggisch, W., 1991. The global Frasnian–Famennian 'Kellwasser event'. Geol. Rundsch. 80, 49–72.

Buggisch, W., Joachimski, M.M., 2006. Carbon isotope stratigraphy of the Devonian of central and southern Europe. Palaeogeogr. Palaeoclimatol. Palaeoecol. 240, 68–88.

Buggisch, W., Mann, U., 2004. Carbon isotope stratigraphy of Lochlovian to Eifelian limestones from the Devonian of central and southern Europe. Geol. Rundsch. (Int. J. Earth Sci.) 93, 521–541.

Cartigny, P., Harris, J.W., Phillips, D., Girard, M., Javoy, M., 1998. Subduction-related diamonds? — The evidence for a mantle-derived origin from coupled $\delta^{13}C$–$\delta^{15}N$ determinations. Chem. Geol. 147, 147–159.

Cartigny, P., Jendrzejewski, N., Pineau, F., Petit, E., Javoy, M., 2001. Volatile (C, N, Ar) variability in MORB and the respective roles of mantle source heterogeneity and degassing: the case of the Southwest Indian Ridge. Earth Planet. Sci. Lett. 194, 241–257.

Chang, S., Berner, R.A., 1999. Coal weathering and the geochemical carbon cycle. Geochim. Cosmochim. Acta 63, 3301–3310.

Coltice, N., Simon, L., Lécuyer, C., 2004. Carbon isotope cycle and mantle structure. Geophys. Res. Lett. 31, L05603. doi:10.1029/2003GL018873.

Dessert, C., Dupré, B., François, L.M., Schott, J., Gaillardet, J., Chakrapani, G., Bajpai, S., 2001. Erosion of Deccan Traps determined by river geochemistry: impact on the global climate and the $^{87}Sr/^{86}Sr$ ratio of seawater. Earth Planet. Sci. Lett. 188, 459–474.

Dessert, C., Dupré, B., Gaillardet, J., François, L.M., Allègre, C.J., 2003. Basalt weathering laws and the impact of basalt weathering on the global carbon cycle. Chem. Geol. 202, 257–273.

Ellwood, B.B., Benoist, S.L., El Hassani, A., Wheeler, C., Crick, R.E., 2003. Impact ejecta layer from the Mid-Devonian: possible connection to global mass extinctions. Science 300, 1734–1737.

Endal, A.S., Sofia, S., 1981. Rotation in solar-type stars, I, evolutionary models for the spin-down of the sun. Astrophys. J. 243, 625–640.

François, L.M., Gérard, J.-C., 1986. A numerical model of the evolution of ocean sulfate and sedimentary sulfur during the last 800 million years. Geochim. Cosmochim. Acta 50, 2289–2302.

François, L.M., Goddéris, Y., 1998. Isotopic constraints on the Cenozoic evolution of the carbon cycle. Chem. Geol. 145, 177–212.

François, L.M., Walker, J.C.G., 1992. Modelling the Phanerozoic carbon cycle and climate: constraints from the $^{87}Sr/^{86}Sr$ isotopic ratio of seawater. Am. J. Sci. 292, 81–135.

Freeman, K.H., Hayes, J.M., 1992. Fractionation of carbon isotopes by phytoplankton and estimates of ancient CO_2 levels. Glob. Biogeochem. Cycles 6, 185–198.

Friedman, W.E., Cook, M.E., 2000. The origin and early evolution of tracheids in vascular plants: integration of palaeobotanical and neobotanical data. Philos. Trans. R. Soc. Lond., B 355, 857–868.

Froelich, P.N., Bender, M.L., Luedtke, N.A., 1982. The marine phosphorus cycle. Am. J. Sci. 282, 474–511.

Gaffin, S., 1987. Ridge volume dependence on sea-floor generation rate and inversion using long-term sea-level change. Am. J. Sci. 287, 596–611.

Gaillardet, J., Dupré, B., Louvat, P., Allègre, C.J., 1999. Global silicate weathering and CO_2 consumption rates deduced from the chemistry of large rivers. Chem. Geol. 159, 3–30.

Goddéris, Y., François, L.M., 1995. The Cenozoic evolution of the strontium and carbon cycles: relative importance of continental erosion and mantle exchange. Chem. Geol. 126, 169–190.

Goddéris, Y., Joachimski, M.M., 2004. Global change in the Late Devonian: modelling the Frasnian–Famennian short-term carbon isotope excursions. Palaeogeogr. Palaeoclimatol. Palaeoecol. 202, 309–329.

Holland, H.D., 1978. Chemistry of the Atmosphere and Oceans. John Wiley & Sons, NY.

Holland, H.D., 1984. The Chemical Evolution of the Atmosphere and Oceans. Princeton Univ. Press, Princeton, NJ.

Joachimski, M., Buggisch, W., 1993. Anoxic events in the Late Frasnian — causes of the Frasnian–Famennian faunal crisis? Geology 21, 675–678.

Joachimski, M.M., Buggisch, W., 2002. Conodont apatite $\delta^{18}O$ signatures indicate climatic cooling as a trigger of the Late Devonian (F–F) mass extinction. Geology 30, 711–714.

Joachimski, M.M., van Geldern, R., Breisig, S., Buggisch, W., Day, J., 2004. Oxygen isotope evolution of biogenic calcite and apatite during the Middle and Late Devonian. Int. J. Earth Sci. (Geol. Rundsch.) 93, 542–553.

Johnson, J.G., 1970. Taghanic onlap and the end of North America Devonian provinciality. Geol. Soc. Amer. Bull. 81, 2077–2105.

Johnson, J.G., Klapper, G.S., Sandberg, C.A., 1985. Devonian eustatic fluctuations in Euramerica. Geol. Soc. Amer. Bull. 96, 567–587.

Johnson, J.G., Klapper, G.S., Elrick, M., 1996. Devonian-transgressive–regressive cycles and biostratigraphy, Northern Antelope Range: establishment of reference horizons for global cycles. Palaios 11, 3–14.

Kampschulte, A., Strauss, H., 2004. The sulfur isotopic evolution of Phanerozoic seawater based on the analysis of structurally substituted sulfate in carbonates. Chem. Geol. 204, 255–286.

Kuhn, T., Ostertag-Henning, Joachimski, M.M., Freeman, K.C., 2001. Changes in the photosynthetic fractionation (ϵ_P) in the Late Palaeozoic. Terra Nostra 2001/4, 35–39.

Leary, R.L., Pfefferkorn, H.W., 1977. An Early Pennsylvanian flora with Megalopteris and Noeggerathiales from West Central Illinois. Ill. State Geol. Surv. 500, 1–77.

Lécuyer, C., Ricard, Y., 1999. Long-term fluxes and budget of ferric iron: implication for the redox states of the Earth's mantle and atmosphere. Earth Planet. Sci. Lett. 165, 197–211.

Lyons, P.C., Darrah, W.C., 1989. Earliest conifers of North America: upland and/or paleoclimatic indicators? Palaios 4, 480–486.

Marty, B., Jambon, A., 1987. $C/^3He$ in volatile fluxes from the solid Earth: Implications for carbon geodynamics. Earth Planet. Sci. Lett. 83, 16–26.

McGhee, G.R., 2001. The 'multiple impacts hypothesis' for mass extinction: a comparison of the Late Devonian and the Late Eocene. Palaeogeogr. Palaeoclimatol. Palaeoecol. 176, 47–58.

Miller, K.G., Kominz, M.A., Browning, J.V., Wright, J.D., Mountain, G.S., Katz, M.E., Sugarman, P.J., Cramer, B.S., Christie-Blick, N., Pekar, S.F., 2005. The Phanerozoic record of global sea-level change. Science 310, 1293–1298.

Mook, W.G., Bommerson, J.C., Staverman, W.H., 1974. Carbon isotope fractionation between dissolved and gaseous carbon dioxide. Earth Planet. Sci. Lett. 22, 169–176.

Mosbrugger, V., 1990. The tree habit in land plants. Springer, Berlin. 161 pp.

Munhoven, G., 1997. Modeling glacial–interglacial atmospheric CO_2 variations: the role of continental weathering. PhD Thesis, University of Liège, Liège.

Murphy, A.E., Sageman, B.B., Hollander, D.J., Lyons, T.W., 2000. Black shale deposition and faunal overturn in the Devonian Appalachian basin: clastic starvation, seasonal water-column mixing, and efficient biolimiting nutrient recycling. In: Huber, B.T., MacLeod, K.G., Wing, S.L. (Eds.), Warm Climates in Earth History. Cambridge University Press, Cambridge, pp. 351–385.

Oliva, P., Viers, J., Dupré, B., 2003. Chemical weathering in granitic environments. Chem. Geol. 202, 225–256.

Opdyke, B.N., Wilkinson, B.H., 1988. Surface area control of shallow cratonic to deep marine carbonate accumulation. Paleoceanograpy 3, 685–703.

Ormiston, A.R., Oglesby, R.J., 1995. Effect of Late Devonian paleoclimate on source rock quality and location. AAPG Stud. Geol. 40, 105–132.

Peters-Kottig, W., Strauss, H., Kerp, H., 2006. The land plant $\delta^{13}C$ record and plant evolution in the late Paleozoic. Palaeogeogr. Palaeoclimatol. Palaeoecol. 240, 237–252.

Petsch, S.T., Berner, R.A., 1998. Coupling the geochemical cycles of C, P, Fe, and S: the effect on atmospheric O_2 and the isotopic records of carbon and sulfur. Am. J. Sci. 298, 246–262.

Petsch, S.T., Berner, R.A., Eglinton, T.I., 2000. A field study of the chemical weathering of ancient sedimentary organic matter. Org. Geochem. 31, 475–487.

Rothwell, G.W., Mapes, G., Mapes, R.H., 1997. Late Palaeozoic conifers of North America: structure, diversity and occurrences. Rev. Palaeobot. Palynol. 95, 95–113.

Royer, D.L., Berner, R.A., Beerling, D.J., 2001. Phanerozoic atmospheric CO_2 change: evaluating geochemical and paleobiological approaches. Earth-Sci. Rev. 54, 349–392.

Sano, Y., Williams, S.N., 1996. Fluxes of mantle and subducted carbon along convergent plate boundaries. Geophys. Res. Lett. 23, 2749–2752.

Sepkoski, J.J., 1996. Patterns of Phanerozoic extinction; a perspective from global databases. In: Walliser, O.H. (Ed.), Global Events and Event Stratigraphy. Springer-Verlag, Berlin, pp. 35–51.

Scotese, C.R., McKerrow, W.S., 1990. Revised world map and introduction. In: McKerrow, W.S., Scotese, C.R. (Eds.), Paleozoic Paleogeography and Biogeography. Geol. Soc. London Mem., vol. 51, pp. 1–21.

Scott, A.C., Chaloner, W.G., 1983. The earliest conifer from the Westphalian B of Yorkshire. Proc. R. Soc. Lond., B 220, 163–182.

Scott, A.C., Glasspool, I.J., 2006. The diversification of Paleozoic fire systems and fluctuations in atmospheric oxygen concentration. Proc. Natl. Acad. Sci. 103, 10861–10865.

Shanks, W.C., Bischoff, J.L., Rosenbauer, R.J., 1981. Seawater sulfate reduction and sulfur isotope fractionation in basaltic systems: interaction of seawater with fayalite and magnetite at 200–350 °C. Geochim. Cosmochim. Acta 45, 1977–1995.

Stein, W.E., Mannolini, F., VanAller Hernick, L., Landing, E., Berry, C.M., 2007. Giant cladoxylopsid trees resolve the enigma of the Earth's earliest forest stumps at Gilboa. Nature 446, 904–907.

Strauss, H., 1997. The isotopic composition of sedimentary sulfur through time. Palaeogeogr. Palaeoclimatol. Paleoecol. 132, 97–118.

Strauss, H., 1999. Geological evolution from isotope proxy signals: sulfur. Chem. Geol. 161, 89–101.

Streel, M., Caputo, M.V., Loboziak, S., Melo, J.H.G., 2000. Late Frasnian–Famennian climates based on palynomorph analyses and the question of the Late Devonian glaciations. Palaeogeogr. Palaeoclimatol. Paleoecol. 52, 121–173.

Thompson, J.B., Newton, C.R., 1988. Late Devonian mass extinction: episodic climatic cooling or warming. In: McMillian, N.J., Embry, A., Glass, D.J. (Eds.), Devonian of the World. Can. Soc. Petrol. Mineral. Mem., vol. 14, pp. 29–34.

Van Cappellen, P., Ingall, E.D., 1996. Redox stabilization of the atmosphere and oceans by phosphorus-limited marine productivity. Science 271, 493–496.

Van Geldern, R., Joachimski, M.M., Day, J., Jansen, U., Alvarez, F., Yolkin, E.A., Ma, X.-P., 2006. Carbon, oxygen and strontium isotope records of Devonian brachiopod shell calcite. Palaeogeogr. Palaeoclimatol. Palaeoecol. 240, 47–67.

Varekamp, J.C., Kreulen, R., Poorfter, R.P.E., Van Berger, M.J., 1992. Carbon sources in arc volcanism, with implications for the carbon cycle. Terra Nova 4, 363–373.

Veizer, J., Ala, D., Azmy, K., Bruckschen, P., Buhl, D., Bruhn, F., Carden, G.A.F., Diener, A., Ebneth, S., Goddéris, Y., Jasper, T., Korte, C., Pawellek, F., Podlaha, O.G., Strauss, H., 1999. $^{87}Sr/^{86}Sr$, d13C and d18O evolution of Phanerozoic seawater. Chem. Geol. 161, 59–88.

Walker, J.C.G., 1986. Global geochemical cycles of carbon, sulfur and oxygen. Mar. Geol. 70, 159–174.

Walliser, O.H., 1996. Global events in the Devonian and Carboniferous. In: Walliser, O.H. (Ed.), Global Events and Event Stratigraphy. Springer-Verlag, Berlin, pp. 225–250.

Wanninkof, R., 1992. Relationship between wind speed and gas exchange over the ocean. J. Geophys. Res. 97, 7373–7382.